PERGAMON

International Journal of Multiphase Flow 28 (2002) 943–961

International Journal of Multiphase Flow

www.elsevier.com/locate/ijmulflow

Liquid entrainment, droplet concentration and pressure gradient at the onset of annular flow in a vertical pipe

J.R. Barbosa Jr. [1], G.F. Hewitt [*], G. König [2], S.M. Richardson

Department of Chemical Engineering and Chemical Technology, Imperial College of Science, Technology and Medicine, Prince Consort Road, London SW7 2BY, UK

Received 23 March 2001; received in revised form 16 December 2001

Abstract

There is a dearth of data on flow parameters in the transition region between churn and annular flow. To address this deficiency, adiabatic air–water experiments were carried out in a vertical test section (31.8 mm internal diameter, 10.8 m long) in which an isokinetic probe was employed to measure the local mass fluxes of gas and of entrained liquid droplets in the core region; pressure gradient was also measured. The tests covered pressures ranging from 1.7 to 5 bara and liquid superficial velocities ranging from 0.012 to 0.33 $m\,s^{-1}$. Average liquid entrained fraction and pressure gradient exhibited minima at gas flow rates that, according to a widely applied flow reversal criterion, correspond to the point of transition to upwards co-current annular flow. Also, the profiles of local droplet concentration characterise churn flow as a region in which the radial gradients of droplet concentration tend to disappear with increasing gas flow rate. As annular flow takes place, the local concentration is virtually constant with respect to radial position and gas flow rate. An empirical correlation is finally proposed for the prediction of liquid entrained fraction at the onset of annular flow. © 2002 Published by Elsevier Science Ltd.

Keywords: Gas–liquid flow; Churn flow; Annular flow; Isokinetic probes; Droplet entrainment

1. Introduction

This paper presents an experimental study on liquid entrainment in the region of transition between the churn and annular flow regimes in vertical gas–liquid flow. Here, churn flow is

[*] Corresponding author. Tel.: +44-20-759-45562; fax: +44-20-759-45564.

E-mail address: g.hewitt@ic.ac.uk (G.F. Hewitt).

[1] Present address: Departamento de Engenharia Mecânica, Universidade Federal de Santa Catarina, UFSC, 88040-900 Florianópolis, SC, Brazil.

[2] On a summer attachment from Institut für Strömungslehre, Universität Karlsruhe, Germany.

0301-9322/02/$ - see front matter
PII: S0301-9322(02)00003-4

defined as the regime occurring after the breakdown of slug flow, where the liquid film is thick, highly oscillatory and swept by large flooding-type waves. The gas core is continuous and there is a considerable amount of liquid entrained as droplets. As the gas flow rate increases, there is a gradual cessation of downwards film flow giving rise ultimately to upwards, unidirectional annular flow.

A series of events which take place at the churn–annular boundary provide a number of possible criteria for correlating this flow pattern transition (Jayanti and Brauner, 1994). Among these, the most common is the flow reversal point criterion. A simple expression to determine this is given by (Hewitt and Wallis, 1963; Wallis, 1969),

$$U_{GS}^{*} = U_{GS}\sqrt{\frac{\rho_G}{g d_T(\rho_L - \rho_G)}} \approx 1, \tag{1}$$

where U_{GS} is the superficial gas velocity, g is the acceleration due to gravity, d_T is the diameter of the tube and ρ_G and ρ_L are the densities of the gas and of the liquid.

Although parameters such as pressure gradient and wall shear stress are well characterised in the churn–annular region (Owen, 1986; Whalley and McQuillan, 1985; Govan et al., 1991), there is a dearth of experimental data on the mass fraction of the liquid flow initially entrained as droplets at the onset of annular flow. This lack of experimental data may exist due to the fact that the complex features of the liquid film in the churn–annular region make the application of experimental techniques that employ film removal devices (porous sinters, slits) very difficult. Azzopardi and Zaidi (2000) pointed out the problems associated with the interpretation of entrainment measurements obtained using porous sinters under such flow conditions.

Most models for annular flow (see for instance Whalley et al., 1974, and Govan, 1990) require a value of entrained fraction at the onset of annular flow as a boundary/initial condition. However, results for heat transfer coefficient and heat flux are not very sensitive to this initial value. Recent studies (Barbosa et al., 2000; Barbosa and Hewitt, 2001a,b) showed that, as opposed to single component systems, the role of the initial entrained fraction is a major one in determining the heat transfer coefficient in annular flow of mixtures. Essentially, the relationship existing between quality and saturation temperature at ideal hydrodynamic equilibrium conditions is broken down by liquid entrainment and local differences in concentration between the liquid film and droplets develop significantly along the channel. This makes the knowledge of the initial conditions for mass conservation in annular flow very important to the correct description of the heat transfer behaviour of mixtures.

As discussed above, the use of techniques that rely on a direct measurement of the film flow rate to determine the entrained fraction in churn flow may fail because of the complexity of the film flow in the churn and churn–annular transition regions. So far, techniques based on the collection of a sample of the droplet flow by means of a probe inserted in the gas core seem to be the only viable ones.

Wallis (1962) used a single, axially located, sampling probe to provide some information on the behaviour of the entrained fraction in the churn–annular flow region. He carried out experiments in a 12.7 mm internal diameter vertical pipe and his results are shown in Fig. 1 for both co-current upflow and downflow conditions. The difference in entrained fraction behaviour between these two cases suggests that there is some entrainment activity associated with the sub-annular region ($U_{GS}^{*} < 1$) in upflow. At what seems to be the region of transition between churn flow and annular

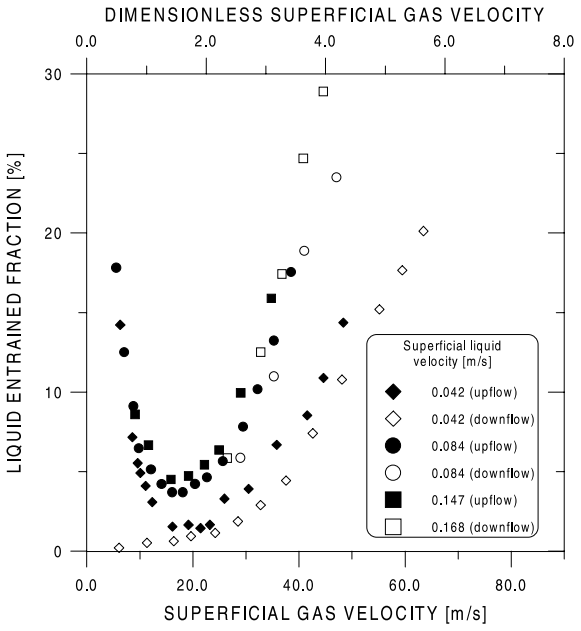

Fig. 1. Variation of entrained fraction with gas velocity (Wallis, 1962).

flow, the entrained fraction goes through a minimum before starting to increase again; a trend remarkably similar to that of the pressure gradient in this same region (Govan et al., 1991).

Gill and co-workers (Gill et al., 1963, 1964) presented a series of studies on the nature of the gas core in annular flow. They made use of a sampling probe (1.57 mm internal diameter) which could be traversed both axially and radially in a 9 m long, 31.8 mm internal diameter vertical pipe. The mass flow rates (mass fluxes) ranged from 0.013 to 0.088 $\mathrm{kg\,s^{-1}}$ (16.3–110.8 $\mathrm{kg\,m^{-2}\,s^{-1}}$) for air and 0.004–0.156 $\mathrm{kg\,s^{-1}}$ (5.0–196.4 $\mathrm{kg\,m^{-2}\,s^{-1}}$) for water. Gill et al. measured the impact pressure on the probe and, by assuming that the droplet–air mixture behaved homogeneously, they obtained the local gas mass flux, $\dot{m}_{\mathrm{G}}$, from measurements of $\dot{m}_{\mathrm{LE}}$ (the droplet collection rate) and of Δp_{i} (the impact pressure).

Gill et al. (1964) observed a different pattern of entrainment flow at low gas flow rates (0.013 $\mathrm{kg\,s^{-1}}$). The entrained liquid mass flux profiles presented flat minima at low gas flow rates whereas at high gas flow rate maxima at all water mass flow rates were observed. They also observed a reversal in the effect of the air rate on entrainment; the data for 0.013 $\mathrm{kg\,s^{-1}}$ of air ($U^{*}_{\mathrm{GS}} \approx 0.67$) showing consistently a higher entrainment than those for 0.026 $\mathrm{kg\,s^{-1}}$ ($U^{*}_{\mathrm{GS}} \approx 1.34$). The entrained fraction would subsequently increase again with increasing gas flow rate. They attributed this behaviour to the proximity to churn flow. Unfortunately, the lack of precision in the readings of impact pressure at low gas flow rates hindered the acquisition of reasonably satisfactory water mass flux profiles.

For co-current annular flow, Gill et al. (1964) found that, apart from the regions very close to the wall, the local droplet concentration, $C(r)$, remained fairly constant across the tube (which is consistent with an assumption of droplet diffusion equilibrium). Furthermore, the local

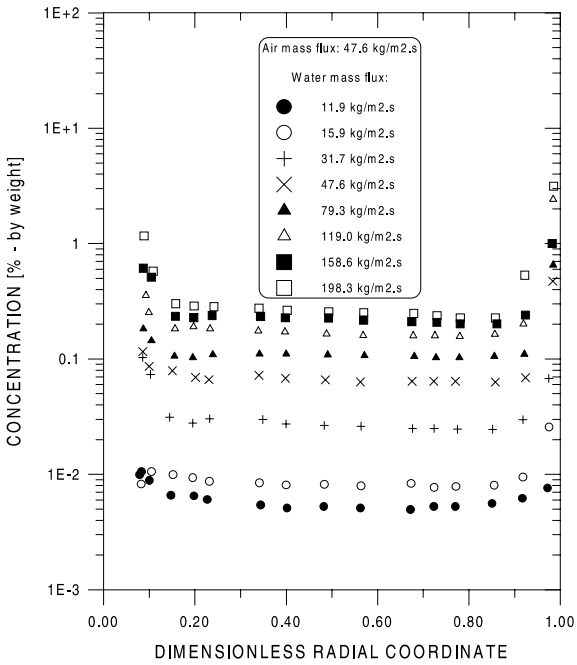

Fig. 2. Droplet concentration distributions in annular flow (Gill et al., 1964).

concentration was virtually independent of the gas flow rate. Typical results are shown in Fig. 2. The local droplet concentration, C, is defined as

$$C(r) = \frac{\rho_G \dot{m}_{LE}(r)}{\rho_L \dot{m}_G(r) + \rho_G \dot{m}_{LE}(r)}, \tag{2}$$

where r is the radial coordinate, and $\dot{m}_{LE}$ and $\dot{m}_G$ are the local entrained liquid and gas mass fluxes (defined as the ratio between the mass flow rates of liquid and gas collected by the probe and the cross-sectional area of the probe).

More recent measurements of entrained fraction were performed by Verbeek et al. (1993), Fore and Dukler (1995) and Azzopardi and Zaidi (2000). Verbeek et al. (1993) investigated the effect of pipe diameter and of physical properties on the entrainment curve. They observed that the minimum in the entrainment curve is shifted to higher gas velocities for large tube diameter (50.8 and 101.6 mm), low surface tension and high liquid viscosity systems. Fore and Dukler (1995) made use of a 50.8 mm internal diameter vertical test section in which two different air–liquid mixtures (with $\eta_L = 1$ and 6 cP respectively, where η_L is the liquid viscosity and 1 cP $= 1 \times 10^{-3}$ Pa s) were employed. For the low viscosity system, the minima of the pressure gradient and entrained fraction distributions took place at $U^*_{GS} \approx 1$. This was in line with previous pressure gradient measurements carried out by Zabaras et al. (1986), who observed minima at $U^*_{GS} = 1.06$ for a wide range of liquid flow rates in a 1 M solution of sodium hydroxide plus 0.005 M potassium ferricyanide and 0.005 M potassium ferricyanide system ($\rho_L = 1020$ kg m^{-3}, $\eta_L = 1.04$ cP). The diameter of the test section employed by Zabaras et al. (1986) was 50.8 mm. For the high viscosity system investigated by Fore and Dukler (1995), the minima of the entrained fraction

curves (but not of the pressure gradient curves) was displaced towards high gas velocities. Unfortunately, for this case, reported gas velocities were not high enough in order to characterise the entrainment curve minima. Azzopardi and Zaidi (2000) carried out experiments in a 38.0 mm internal diameter vertical test section and determined the liquid entrained fraction for $U^*_{GS} \geqslant 1$ over a wide range of conditions.

The objective of the present study is to investigate in further detail the behaviour of entrainment related parameters in the churn–annular regime by making extensive measurements of localised mass fluxes of gas and liquid in the core region. To achieve that, an *isokinetic probe* is employed so that simultaneous measurements of the entrained liquid and gas streams can be carried out. The experiments were performed in a vertical, adiabatic, air–water facility. The internal diameter of the test section is 31.8 mm and the pipe length between the liquid inlet and the measurement position is 10.8 m. Experimental conditions were such that a considerable range of total liquid mass fluxes (15–350 $\mathrm{kg\,m^{-2}\,s^{-1}}$) and pressures (2–5 bara) was covered. Typically, the gas mass fluxes were such that U^*_{GS} ranged from 0.5 to 1.7 (a value that is well into fully developed annular flow). Measurements of pressure gradient were also undertaken.

In what follows, Section 2 describes the experimental apparatus and procedure for measurements of entrained liquid fraction, droplet concentration and of pressure gradient. Results are shown in Section 3. Also, an empirical correlation for entrained fraction at the onset of annular flow is proposed. Conclusions are drawn in Section 4.

2. Experimental apparatus

2.1. The long tube system facility

A schematic diagram of the long tube system (LOTUS) air–water facility is shown in Fig. 3. The test section used in the facility consists of a 31.8 mm internal diameter vertical copper tube. The tube is made up of sections of various lengths which were attached to an accurately aligned vertical fixed beam.

Air supplied from the site mains at approximately 7.5 bara is fed to the bottom of the tube via a large radius U-bend and and metered using a differential pressure transducer connected to an orifice plate. Water is pumped through the system using a 1.5 kW pump. The water flow rate is metered using calibrated rotameters. The water was introduced into the tube through a porous wall (sinter) section. The distance between this entrance and the measurement position was 10.8 m.

The test spool containing the isokinetic probe mounting block, a short transparent section for visualisation and the tappings for pressure drop measurement is located at the top end of the long tube test section. After leaving the test section, the flow is returned to the main water tank through a separator. The air is vented to the atmosphere.

2.2. Pressure gradient measurement

The pressure gradient was evaluated by measuring the pressure drop between two points along the test section. A differential pressure transducer (Druck PMP4170) connected to two pressure

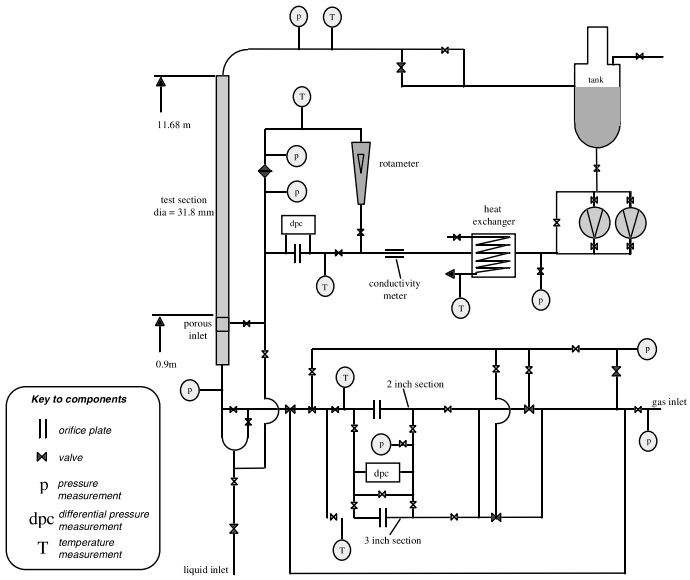

Fig. 3. Schematic diagram of the LOTUS facility.

tappings (3 mm internal diameter) was used for such a measurement. An absolute pressure transducer (Druck PMP4171) was also connected to one of the tappings. The distance between the tappings is 830 ± 1 mm. To avoid ambiguities in the pressure drop measurements associated with the presence of two phases in the tapping lines a liquid purge system (0.1–1% of the total liquid flow rate) was installed.

The signals from the absolute and differential pressure transducers were sent to a computer equipped with a data acquisition card. The sampling frequency was 1000 Hz and the data averaged over a period of approximately 10 s.

2.3. The isokinetic probe technique

2.3.1. Working principle

The isokinetic sampling technique is based on a single probe which is similar in structure to a Pitot-static tube, but with a pressure tapping at the mouth which measures the difference between the pressure in the mouth of the probe and the static pressure in the flow channel. The probe is mounted with its mouth facing the flow and the oncoming fluid is collected at a controlled rate. The rate of collection can be regulated so that the fluids enter the probe in the same mixture proportions and at the same velocities as the flow would have in the absence of the probe. This *isokinetic* behaviour is achieved by establishing a collection rate which gives a null difference between the apparent dynamic pressure and the static pressure near the mouth of the probe, a condition indicating that the velocity upstream and within the probe are identical.

The measured pressure difference when the collection rate is zero is the actual dynamic pressure of the fluid stream (as in a Pitot-tube). There have been a number of models for interpretation of

Table 1
Dimensions of the isokinetic sampling probe

Tube	Outer diameter (mm)	Inner diameter (mm)	Wall thickness (mm)
Sampling	6.35	5.842	0.254
Wall static pressure	1.588	1.181	0.201
Probe static pressure	1.588	1.181	0.201

such pressures in two-phase flow. However, in order to use this impact pressure measurement to obtain local information about the flow (e.g. slip), an independent assessment of the local void fraction, ε_G, is required. As simultaneous measurements of ε_G were not made in the present study, the probe was never operated under zero collection rate conditions.

2.3.2. The probe

The isokinetic probe used in the present work is identical to that designed and used by Khor (1998). The probe is made of stainless steel and its main dimensions are given in Table 1. The horizontal length of the probe is 180 mm and the vertical stem is 300 mm. The sampling probe could be traversed across the pipe cross-section by means of a screw turning mechanism. A fine thread screw adjustment allowed the probe to be positioned with an accuracy of approximately ± 0.2 mm.

In the probe design exercise, Khor (1998) concluded that the pressure difference between the throat and the inside (probe static) tapping position was negligible. The ratio between the probe outer diameter and the pipe diameter is 0.2 and it is therefore likely that the presence of the probe significantly affects the flow in the probe surroundings. Nevertheless, when the probe is operated at isokinetic conditions, the disturbances due to the probe are negligible and a measurement of the true flow conditions which would be present in the absence of the probe are achieved.

2.3.3. Measurement arrangement

The system for collection of entrained liquid and gas mass fluxes is schematically presented in Fig. 4. The two-phase sample collected by the probe is diverted via a three-way valve into an acrylic resin gas–liquid separator. From the separator, the gas flowed to a calibrated rotameter. The liquid was accumulated in the separator for a given time interval (measured using a digital chronometer with an uncertainty of ± 0.05 s). After each measurement, the collected liquid was drained from the separator into a container whose weight was measured with an uncertainty of ± 0.005 kg before and after each collection. The collected liquid flow rate is given by the ratio between the weight of the collected liquid and the collection time interval.

The isokinetic operation condition was obtained by adjusting the manual needle valve until the difference between probe static pressure and the wall static pressure was zero. The probe tappings were connected to a pressure transducer (Rosemount 3051C) which was set to operate within the range -200 to 400 Pa. The electrical signal from the transducer was amplified (range 2–10 V) and then sent to a digital bench voltmeter (Keithley 195A). The voltmeter was equipped with filtering devices which were used to damp the severe signal fluctuations associated with churn flow. The uncertainty in the voltmeter reading was ± 0.01 V, which corresponded to ± 0.75 Pa.

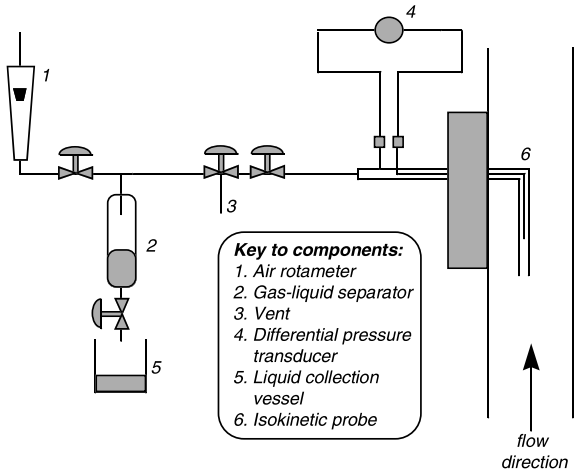

Fig. 4. Experimental setup for gas and liquid collection using the isokinetic sampling probe.

To ensure that the measurements were unambiguous, the pressure tappings on the probe were kept free of liquid by purging the lines of the differential pressure transducer with compressed air available from the site mains.

2.4. Entrained fraction measurement

The mass flow rate of liquid entrained as droplets, $\dot{M}_{\mathrm{LE}}$, is calculated through an integration of the local entrained liquid mass flux profile over the area of the gas core. This integration has the difficulty that, as the probe approaches the liquid film it intercepts waves on the film which may be wrongly ascribed to entrainment. Here, a procedure for extrapolation/integration of the entrained liquid mass flux profiles developed by Asali et al. (1985) was implemented. It was found that 11% was a representative value for the error (difference between the extrapolated and not extrapolated profiles) associated with this procedure. Further details are given by Barbosa (2001).

The entrained fraction is defined as

$$e = \frac{\dot{M}_{\mathrm{LE}}}{\dot{M}_{\mathrm{L}}}. \tag{3}$$

The insensitivity of the liquid collection rate to changes in air rate through the probe is illustrated in Fig. 5. The probe's high droplet capture efficiency over a wide range of gas extraction rates can be observed. The isokinetic air rate is also shown.

2.5. Experimental procedure

The procedure for the data acquisition is as follows. The test section pressure and the total liquid flow rate are set at the desired values. The flow pressure drop is measured and the pressure gradient calculated. The isokinetic probe is traversed radially and sampling is carried out at three different radial positions. At each radial station, measurements of entrained liquid mass flux and

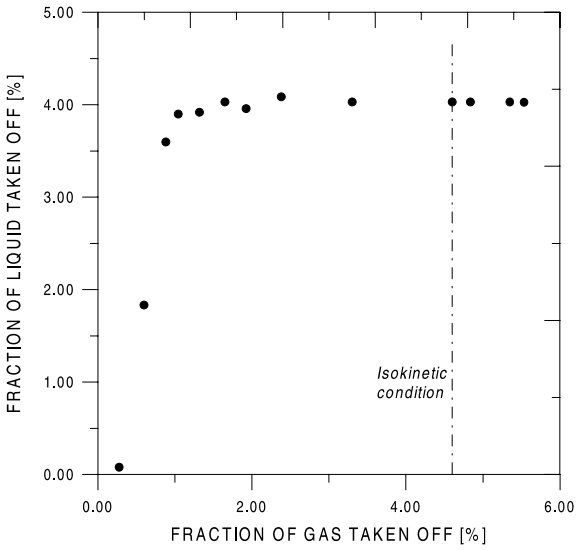

Fig. 5. Liquid collection rate versus air rate through the probe, experimental conditions: $p = 3$ bara, $\dot{m}_L = 45$ kg m^{-2} s^{-1}, $U^*_{GS} = 1.3$.

of isokinetic gas flow rate are carried out. The collection time of entrained liquid at the separator is never less than 8 min for each position. After that, the air flow rate is set at another value and measurements are repeated after steady-state conditions have been reached. Increasing and decreasing gas flow rate runs were performed and no significant difference in the results was observed.

3. Results

3.1. Entrained fraction and pressure gradient

Typical variations of pressure gradient and entrained liquid fraction (Eq. (3)) with the dimensionless gas velocity, U^*_{GS}, are shown in Figs. 6 and 7. The minima of each curve occur at $U^*_{GS} \approx 1$, which coincides with the criterion for flow reversal (Eq. (1)). These trends were observed throughout the range of conditions investigated.

One can justify the occurrence of a minimum in the liquid entrained fraction distributions in the churn–annular region based on the mechanisms by which droplets are generated from interfacial waves. From measurements of drop sizes and from flow visualisation experiments, Azzopardi (1983) identified two mechanisms by which droplet entrainment takes place. In the first mechanism (bag break-up), the gas apparently 'undercuts' a large wave forming and open-ended bubble with a thick filament rim. When this bubble bursts, a rapid transient acceleration of the gas phase accelerates the droplets. In the second mechanism (ligament break-up), the crests of the waves are pulled forward in the form of ligaments, then these ligaments are broken into drops. Azzopardi correlated the occurrence of each one of the mechanisms of droplet formation in annular flow to a

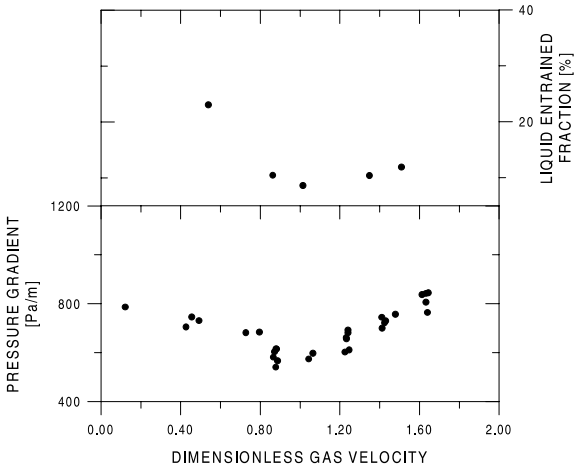

Fig. 6. Entrainment and experimental pressure gradient in the churn–annular region: $p = 2$ bara, $\dot{m}_L = 47\ \mathrm{kg\,m^{-2}\,s^{-1}}$ (nominal).

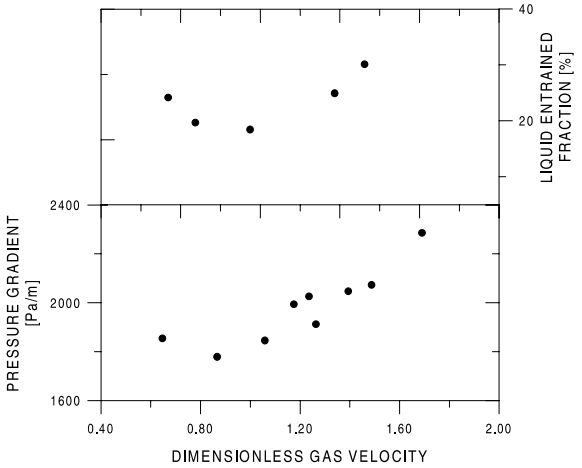

Fig. 7. Entrainment and experimental pressure gradient in the churn–annular region: $p = 2$ bara, $\dot{m}_L = 138\ \mathrm{kg\,m^{-2}\,s^{-1}}$ (nominal).

critical Weber number. By assuming a wave height to mean film thickness ratio of approximately 3.5, good agreement with the transition boundary was found for

$$We = \frac{\rho_G U_{GS}^2 \delta_w}{\sigma} = 25, \tag{4}$$

where δ_w is the wave height and σ is the surface tension.

James et al. (1980) carried out experimental and analytical studies on the motion of droplets in two-phase flow. As a result of their visualisation work (using a laser axial view technique), James et al. found that larger droplets (>200 μm), formed mainly from *bag break-up*, tend to travel in

straight lines at velocities similar to those at the time of their formation. Moreover, droplets formed by ligament break-up tend to stay in the core for much longer due to turbulent eddy interactions within the gas core. James et al.'s final conclusion was that both the direct impaction and the turbulent eddy interaction mechanisms are likely to be important in most practical situations, with droplets of the latter category contributing as much as 70% of the entrained fraction.

Based on the information above, one can retrace the entrainment curve in the light of the mechanisms of droplet formation. At low gas velocities the droplets are generated from the large flooding-type waves through the undercutting (bag break-up) mechanism. These droplets redeposit very quickly on the film. As the gas flow rate is increased and the occurrence of large flooding-type waves subsides, droplets cease to be generated by the (low gas velocity) undercutting mechanism, thus decreasing entrainment. With further and continuous increase of the gas flow rate, disturbance waves start to appear and both mechanisms may coexist, with the filament break-up mechanism gaining greater importance.

Figs. 8 and 9 illustrate the behaviour of the entrained liquid fraction with increasing total liquid flow rate. Error bars are shown and, for the lower liquid mass fluxes, uncertainties are higher mainly due to liquid evaporation (air humidification). As observed in these plots, the liquid entrained fraction decreases with increasing U^*_{GS} in the region of transition between churn flow and annular flow. It starts to increase again when the co-current annular region is entered. The entrained fraction at the minimum region is always higher for the higher total liquid flow rates. As will be seen from Figs. 8 and 9, the fraction of the liquid flow which is entrained appears to be higher for lower liquid flow rates at the lowest dimensionless gas velocities. This trend is not, of course, observed in annular flow, where the fraction entrained generally increases with increasing liquid flow. This probably reflects a change in the liquid entrainment mechanism from the 'bag break-up' mechanism to the 'ligament tearing' mechanism as discussed by Azzopardi (1983). It

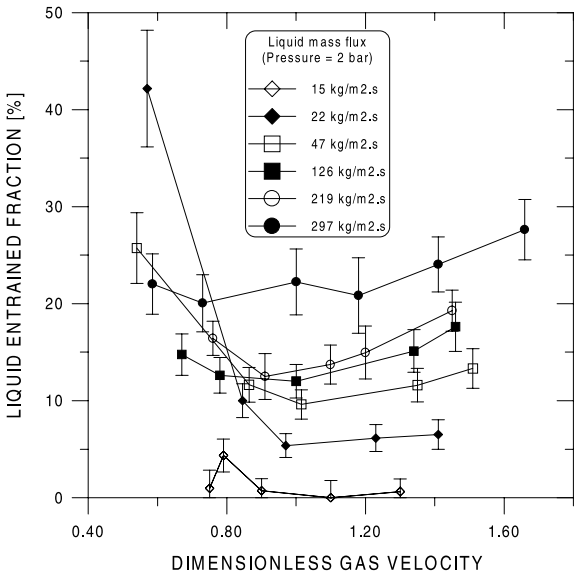

Fig. 8. Liquid entrained fraction as a function of the total liquid mass flux: $p = 2$ bara (nominal).

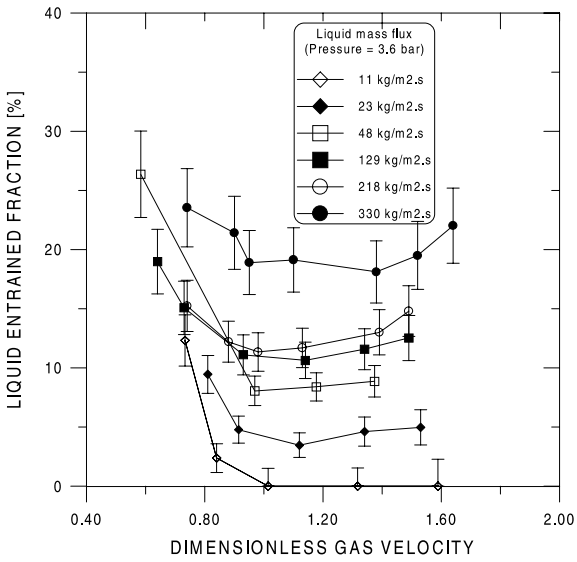

Fig. 9. Liquid entrained fraction as a function of the total liquid mass flux: $p = 3.6$ bara (nominal).

seems likely that a larger proportion of the total liquid flow is present as large waves at the lower liquid flow rates, increasing (proportionally) the propensity for entrainment. Of course, if the results are plotted in terms of entrained flow rate rather than entrained fraction, the reversed trend is not seen.

The effect of pressure on the liquid entrained fraction is illustrated in Figs. 10 and 11. The liquid entrained fraction is virtually constant in the churn region and the differences, though not very pronounced, develop in the annular region. A small suppression of entrainment is obtained with increasing pressure. This is reasonably consistent with previous work, for instance that of Owen (1986).

3.2. Droplet concentration

Profiles of local concentration (Eq. (2)) against a dimensionless radial coordinate, y/d_T, where y is measured from the pipe wall, are shown in Figs. 12 and 13. As the superficial gas velocity increases and annular flow is approached (with U^*_{GS} tending to 1), the radial gradients are smoothed and the local concentration asymptotically approaches a constant value. The difference in concentration profiles observed in churn–annular and annular flow probably reflects the change between 'bag break-up' and 'ligament tearing' mechanisms for entrainment between the two regimes.

Another view of the effect of gas flow rate on entrainment is provided by an analysis of the volumetric flow ratio in the gas core (or the apparent mean concentration), β. It is defined as (Gill et al., 1964),

$$\beta = \frac{\dot{M}_{LE}\rho_G}{\dot{M}_G\rho_L}. \tag{5}$$

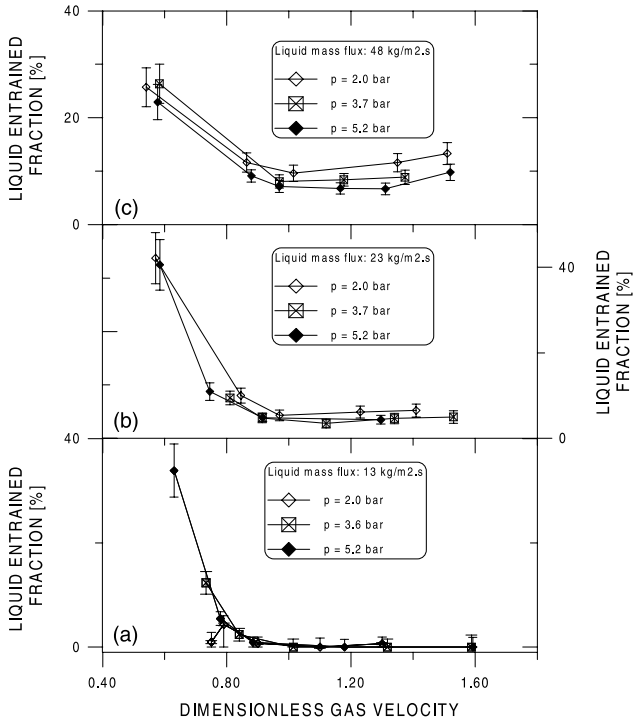

Fig. 10. Liquid entrained fraction as a function of the absolute pressure: (a) $\dot{m}_L = 13\ \mathrm{kg\,m^{-2}\,s^{-1}}$ (nominal), (b) $\dot{m}_L = 23\ \mathrm{kg\,m^{-2}\,s^{-1}}$ (nominal), (c) $\dot{m}_L = 48\ \mathrm{kg\,m^{-2}\,s^{-1}}$ (nominal).

The variation of β with the liquid mass flux is illustrated in Fig. 14. As previously observed by Gill et al. (1964), the data for U^*_{GS} greater than 1.0 fall approximately on a continuous curve with little deviation resulting in variations in air flow rate. The results for $U^*_{GS} < 1$ lie above the line; characterising the increase in entrainment associated with churn flow.

3.3. Measurement uncertainty considerations

Single phase air runs were performed prior to the main series of experiments in order to evaluate the performance of the probe system. Under isokinetic conditions, average velocities were reproducible with an uncertainty of 5% for a wide range of air flow rates and pressures.

In order to ensure the validity of the experimental technique, comparisons with experimental results obtained using a porous (sintered) section (100 mm long) mounted on the test section were carried out. The experiments were performed at sufficiently high gas superficial velocities, where the film flow is unidirectional and the film removal technique can be applied. The mass flux of entrained liquid was obtained from a deduction of the measured film flow rate from the total liquid flow rate. The results obtained from the two techniques are shown in Table 2. The agreement between the two measurement methods is rather good.

After a theoretical investigation of evaporation (air humidification) effects, it was concluded that at low liquid flow rates these are significant and together with the uncertainty in the film flow

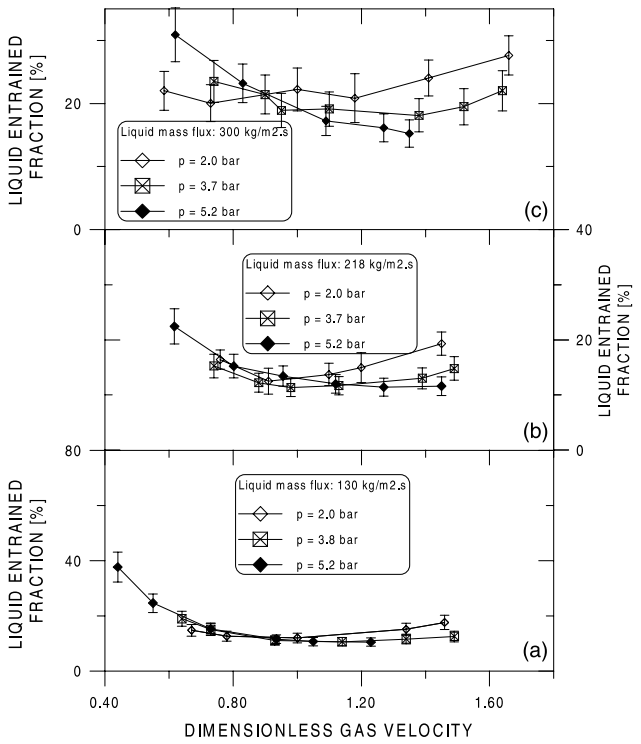

Fig. 11. Liquid entrained fraction as a function of the absolute pressure: (a) $\dot{m}_L = 130\ \mathrm{kg\,m^{-2}\,s^{-1}}$ (nominal), (b) $\dot{m}_L = 218\ \mathrm{kg\,m^{-2}\,s^{-1}}$ (nominal), (c) $\dot{m}_L = 300\ \mathrm{kg\,m^{-2}\,s^{-1}}$ (nominal).

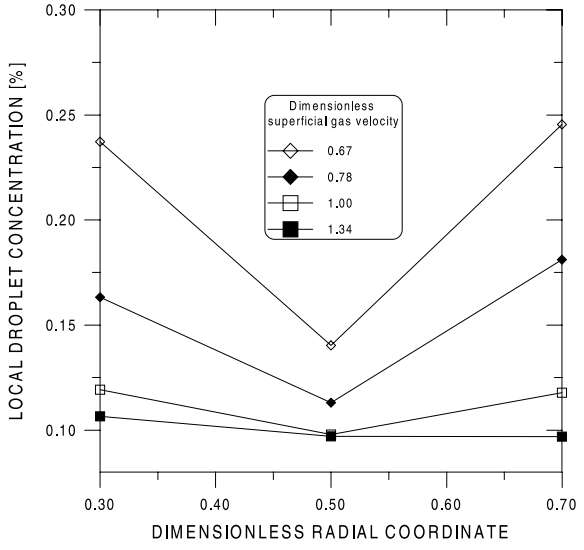

Fig. 12. Profiles of local droplet concentration: $p = 2.1$ bara, $\dot{m}_L = 126.3\ \mathrm{kg\,m^{-2}\,s^{-1}}$.

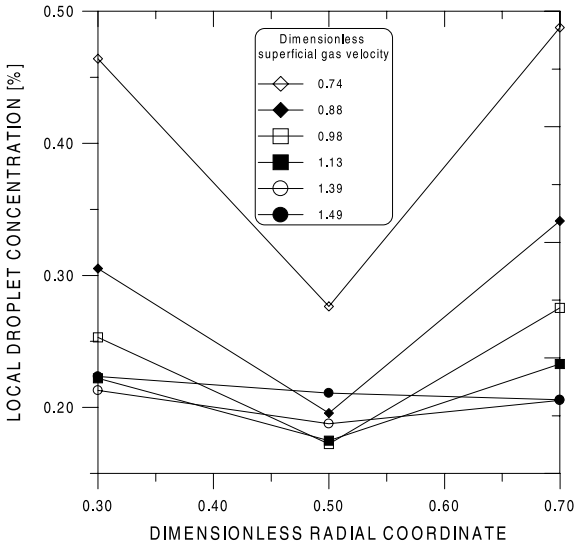

Fig. 13. Profiles of local droplet concentration: $p = 3.7$ bara, $\dot{m}_L = 216.0\ \mathrm{kg\,m^{-2}\,s^{-1}}$.

rate measurement as well as the uncertainty in the input liquid rate can account for most of the apparent entrainment at very low liquid flow rates (error bars in Figs. 8 and 9). The results from this analysis are also in line with an experimental assessment of such effects reported by Azzopardi and Zaidi (2000).

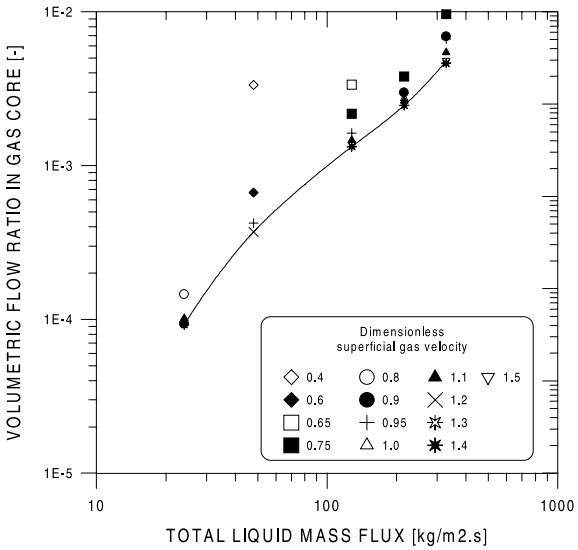

Fig. 14. Volumetric flow ratio: $p = 3.6$ bara (nominal).

Table 2
A comparison of entrained fraction obtained using a porous sinter and the isokinetic probe

U_G^* (–)	$\dot{m}_L$ (kg m^{-2} s^{-1})	$e\%_{sinter}$ (–)	$e\%_{probe}$ (–)
1.2	47	8.84	8.40
1.3	22	4.28	4.62
1.4	48	9.79	8.87
1.5	23	4.95	4.97

3.4. A correlation for entrained fraction

An empirical correlation has been developed for the prediction of the fraction of liquid entrained as droplets at the onset of annular flow, e_{OA}. This is as follows (parameters in SI Units),

$$e_{OA}\% = 0.95 + 342.55\sqrt{\frac{\rho_L \dot{m}_L}{\rho_G \dot{m}_G}}d_T^2. \tag{6}$$

Eq. (6) is valid for $0.9 < U_{GS}^* < 1.3$, $11 < \dot{m}_L < 334$ (in kg m^{-2} s^{-1}), $1.33 < p < 5.2$ (in bara) and $0.0127 < d_T < 0.0508$ (in m). The overall error is approximately equal to $\pm 18.9\%$. Fig. 15 illustrates the prediction of the experimental entrained fraction at the onset of annular flow. As seen in Fig. 15, data from other sources are also well correlated. It is interesting to notice the effect of tube diameter on e_{OA}. The data of Fore and Dukler (1995) and Verbeek et al. (1993) ($d_T = 0.0508$ m) exhibit the highest values of entrained fraction, whereas those of Wallis (1962) ($d_T = 0.0127$ m) are amongst the lowest e_{OA}.

In annular flow models, a common assumption has been that the entrained fraction at the onset of annular flow corresponds to that for hydrodynamic equilibrium, i.e., to equality of deposition

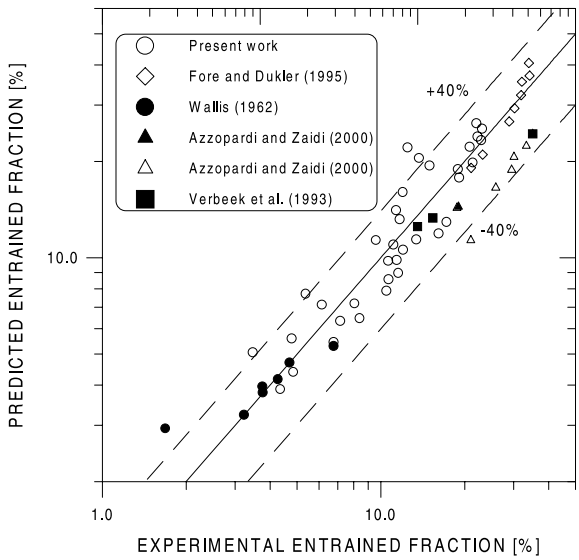

Fig. 15. Prediction of entrained fraction using the proposed correlation.

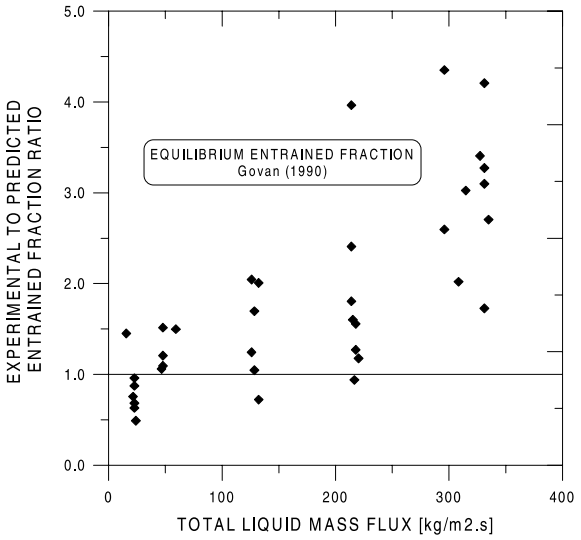

Fig. 16. A comparison between experimental and predicted equilibrium entrained fraction using the droplet interchange correlations of Govan (1990) under hydrodynamic equilibrium conditions.

and entrainment rates, with these rates being predicted from correlations for annular flow. An example of this approach is that of Govan (1990). Fig. 16 shows a comparison between entrained fraction calculated by this approach (using the entrainment and deposition correlations of Govan, 1990) and the actual values measured in the present investigation. As will be seen, there are considerable differences between the measured values and those calculated assuming annular flow equilibrium. It is likely that the flow will be close to equilibrium (after 10.4 m or 325 pipe diameters) and the reason for the discrepancies observed, especially at higher flow rates ($\dot{m}_L > 100$ kg m^{-2} s^{-1}), probably lie in the fact that correlations for entrainment and deposition rates for annular flow do not account for the proximity to churn flow in the transition region and the increase in entrainment associated with it.

4. Conclusions

This paper presents experimental data for droplet entrainment and pressure gradient for the transition region between churn flow and annular flow in a vertical pipe. An isokinetic probe system was used to measure the local distributions of liquid and gas mass fluxes. The main conclusions arising from this study are as follows:

1. In the fully co-current annular region ($U^*_{GS} > 1$), the local droplet concentration is virtually constant within the gas core. In contrast, in the region of transition between churn flow and annular flow the droplet concentration varies across the core, with the sharp radial gradients gradually disappearing with increases in gas velocity towards the annular flow transition.

2. Both pressure gradient and entrained fraction exhibit a minimum at $U^*_{GS} \approx 1$, before increasing again in the annular regime. An explanation for such a behaviour may by sought based on the mechanisms by which droplets are created from interfacial waves present on a liquid film (Azzopardi, 1983). Other features of the behaviour of the entrained fraction could be observed, namely (i) the entrained liquid flow rate (and the entrained fraction) increases with the total liquid flow rate; (ii) the effect of pressure on the entrained fraction is not as pronounced as that of the liquid flow rate, however the pressure seems to affect more the results in the annular flow region (for higher pressures, the entrained fraction increases less with pressure after the minimum is reached); (iii) for low water flow rates ($\dot{m}_L \approx 10\ kg\,m^{-2}\,s{-}1$ and $\dot{m}_L \approx 20\ kg\,m^{-2}\,s{-}1$) the higher uncertainty in the experimental data is attributed to evaporation of the liquid film (air humidification).
3. An empirical correlation was devised to predict the entrained fraction at the onset of annular flow ($0.9 < U^*_{GS} < 1.3$). The correlation predicts data from the present study and from other sources with reasonable accuracy.
4. If an annular flow model is used to predict entrained fraction flow by assuming equilibrium between deposition and entrainment rates predicted by the model, the entrained fraction was severely underestimated for $\dot{m}_L > 100\ kg\,m^{-2}\,s^{-1}$. This can be ascribed to deficiencies of annular flow deposition and entrainment correlations in describing the transition region
5. Further experiments are needed to investigate in more detail the role of physical properties (liquid viscosities and surface tension) on entrainment in the transition region.

Acknowledgements

One of us (JRB) thanks the Brazilian National Research Council (CNPq - Conselho Nacional de Desenvolvimento Científico e Tecnológico) for the award of a scholarship (grant no. 200085/97-2).

References

Asali, J.C., Leman, W., Hanratty, T.J., 1985. Entrainment measurements and their use in design equations. Physicochem. Hydrodyn. 6 (1/2), 207–221.

Azzopardi, B.J., 1983. Mechanisms of entrainment in annular two-phase flow. UKAEA Report AERE-R 11068.

Azzopardi, B.J., Zaidi, S.H., 2000. Determination of entrained fraction in vertical annular gas–liquid flow. J. Fluids Engng. 122, 146–150.

Barbosa Jr., J.R., 2001. Phase change of single component fluids and mixtures in annular flow, Ph.D. thesis, University of London, Imperial College, UK.

Barbosa Jr., J.R., Kandlbinder, T., Hewitt, G.F., 2000. A study of dryout in annular flow of single component hydrocarbons and their mixtures. Multiphase Science and Technology. 12 (314), 265–293.

Barbosa Jr., J.R., Hewitt, G.F., 2001a. Forced convective boiling of binary mixtures in annular flow. Part I: Liquid phase mass transport. Int. J. Heat Mass Transfer 44, 1465–1474.

Barbosa Jr., J.R., Hewitt, G.F., 2001b. Forced convective boiling of binary mixtures in annular flow. Part II: Heat and mass transfer. Int. J. Heat Mass Transfer 44, 1475–1484.

Fore, L.B., Dukler, A.E., 1995. Droplet deposition and momentum transfer in annular flow. AIChE J. 41 (9), 2040–2046.

Gill, L.E., Hewitt, G.F., Hitchon, J.W., Lacey, P.M.C., 1963. Sampling probe studies of the gas core in annular two-phase flow. Part I: The effect of length on phase and velocity distribution. Chem. Eng. Sci. 18, 525–535.

Gill, L.E., Hewitt, G.F., Lacey, P.M.C., 1964. Sampling probe studies of the gas core in annular two-phase flow. Part II: Studies of the effect of phase flow rates on phase and velocity distribution. Chem. Eng. Sci. 19, 665–682.

Govan, A.H., 1990. Modelling of vertical annular and dispersed two-phase flows, Ph.D. thesis, University of London, Imperial College, UK.

Govan, A.H., Hewitt, G.F., Richter, H.J., Scott, A., 1991. Flooding and churn flow in vertical pipes. Int. J. Multiphase Flow 17, 27–44.

Hewitt, G.F., Wallis, G.B., 1963. Flooding and associated phenomena in falling film in a vertical tube. In: Proceedings of Multi-Phase Flow Symposium, Philadelphia, PA, 17–22 November, pp. 62–74.

James, P.W., Hewitt, G.F., Whalley, P.B., 1980. Droplet motion in two-phase flow. UKAEA Report AERE-R 9711.

Jayanti, S., Brauner, N., 1994. Churn flow. In: Hewitt, G.F., Delhaye, J.M., Zuber, N., Kim, J.H.Lahey Jr., R.T. (Eds.), Multiphase Science and Technology, Volume 8—Two-Phase Flow Fundamentals. Begell House Inc., New York.

Khor, S.H., 1998. Three-phase liquid–liquid–gas stratified flow in pipelines. Ph.D. thesis, University of London, Imperial College, UK.

Owen, D.G., 1986. An experimental and theoretical analysis of equilibrium annular flows. Ph.D. thesis, University of Birmingham, UK.

Verbeek, P.H.J., Miesen, R., Schellenkens, C.J., 1993. Liquid entrainment in annular dispersed upflow. European Two-Phase Flow Group Meeting, Hannover, 7–10 June.

Wallis, G.B., 1962. The onset of droplet entrainment in annular gas–liquid flow. General Electric Report No. 62 GL127.

Wallis, G.B., 1969. One-Dimensional Two-Phase Flow. McGraw-Hill, New York.

Whalley, P.B., Hutchinson, P., Hewitt, G.F., 1974. The calculation of critical heat flux in forced convective boiling. Fifth International Heat Transfer Conference, Tokyo, Japan, Paper B6.11.

Whalley, P.B., McQuillan, K.W., 1985. The development and use of a directional wall shear stress probe. Proceedings of the Second International Conference on Multiphase Flow, London, UK, pp. 317–323.

Zabaras, G., Dukler, A.E., Maron, D.M., 1986. Vertical upward cocurrent gas-liquid annular flow. AIChE J. 32 (5), 829–843.